Earth and Planetary Science Letters 381 (2013) 147–155

Contents lists available at ScienceDirect

Earth and Planetary Science Letters

www.elsevier.com/locate/epsl

Large earthquake rupture process variations on the Middle America megathrust

Lingling Ye [a], Thorne Lay [a,*], Hiroo Kanamori [b]

[a] Department of Earth and Planetary Sciences, University of California Santa Cruz, Santa Cruz, CA 95064, USA
[b] Seismological Laboratory, California Institute of Technology, Pasadena, CA 91125, USA

ARTICLE INFO

Article history:
Received 24 April 2013
Received in revised form 14 August 2013
Accepted 19 August 2013
Available online xxxx
Editor: P. Shearer

Keywords:
Middle America earthquakes
Central America forearc sliver
tsunami earthquakes
seismic coupling

ABSTRACT

The megathrust fault between the underthrusting Cocos plate and overriding Caribbean plate recently experienced three large ruptures: the August 27, 2012 (M_w 7.3) El Salvador; September 5, 2012 (M_w 7.6) Costa Rica; and November 7, 2012 (M_w 7.4) Guatemala earthquakes. All three events involve shallow-dipping thrust faulting on the plate boundary, but they had variable rupture processes. The El Salvador earthquake ruptured from about 4 to 20 km depth, with a relatively large centroid time of ~19 s, low seismic moment-scaled energy release, and a depleted teleseismic short-period source spectrum similar to that of the September 2, 1992 (M_w 7.6) Nicaragua tsunami earthquake that ruptured the adjacent shallow portion of the plate boundary. The Costa Rica and Guatemala earthquakes had large slip in the depth range 15 to 30 km, and more typical teleseismic source spectra. Regional seismic recordings have higher short-period energy levels for the Costa Rica event relative to the El Salvador event, consistent with the teleseismic observations. A broadband regional waveform template correlation analysis is applied to categorize the focal mechanisms for larger aftershocks of the three events. Modeling of regional wave spectral ratios for clustered events with similar mechanisms indicates that interplate thrust events have corner frequencies, normalized by a reference model, that increase down-dip from anomalously low values near the Middle America trench. Relatively high corner frequencies are found for thrust events near Costa Rica; thus, variations along strike of the trench may also be important. Geodetic observations indicate trench-parallel motion of a forearc sliver extending from Costa Rica to Guatemala, and low seismic coupling on the megathrust has been inferred from a lack of boundary-perpendicular strain accumulation. The slip distributions and seismic radiation from the large regional thrust events indicate relatively strong seismic coupling near Nicoya, Costa Rica, patchy zones of strong seismic coupling in the shallowest megathrust region along Nicaragua and El Salvador, and small deeper patchy zones of strong seismic coupling near Guatemala, which can be reconciled with the geodetic observations as long as the strong coupling is limited to a small fraction of the megathrust area.

1. Introduction

The Middle America subduction zone (Fig. 1) is distinctive in having pronounced forearc translation parallel to the trench despite the lack of strong obliquity of the plate convergence direction along much of the plate boundary. The extensive GPS data collected over the past two decades (Alvarado et al., 2011; Alvarez-Gomez et al., 2008; Correa-Mora et al., 2009; DeMets, 2001; Franco et al., 2012; Guzman-Speziale and Gomez-Gonzales, 2006; LaFemina et al., 2009; Lyon-Caen et al., 2006; Rodriguez et al., 2009; Turner III et al., 2007) indicate forearc trench-parallel motions along Nicaragua and El Salvador relative to a fixed Caribbean plate have a velocity of 14–15 ± 2 mm/yr toward the diffuse triple junction between the Cocos (CO), Caribbean (CA) and North America (NA) plates. The geodetic observations also indicate very little trench-perpendicular ground velocity that would be expected if the offshore megathrust boundary is locked and significant upper plate convergent strain accumulating.

These geodetic observations have led to the notion of a relatively rigid forearc sliver, or Middle America microplate, extending all the way from Costa Rica to Guatemala. During at least the last several decades of GPS measurements there appears to be very weak interplate coupling between the CO plate and the CA plate forearc sliver along El Salvador and Nicaragua with, at most, limited regions of strong megathrust coupling located offshore of Guatemala and southern Nicaragua. To account for the block-like motion of the forearc sliver in the presence of weak interplate coupling and lack of oblique convergence offshore of El Salvador and southeastern Guatemala, the driving force for the sliver has been attributed to the Cocos Ridge collision with the

* Corresponding author. Tel.: +831 459 3164.
E-mail address: tlay@ucsc.edu (T. Lay).

0012-821X/$ – see front matter
http://dx.doi.org/10.1016/j.epsl.2013.08.042

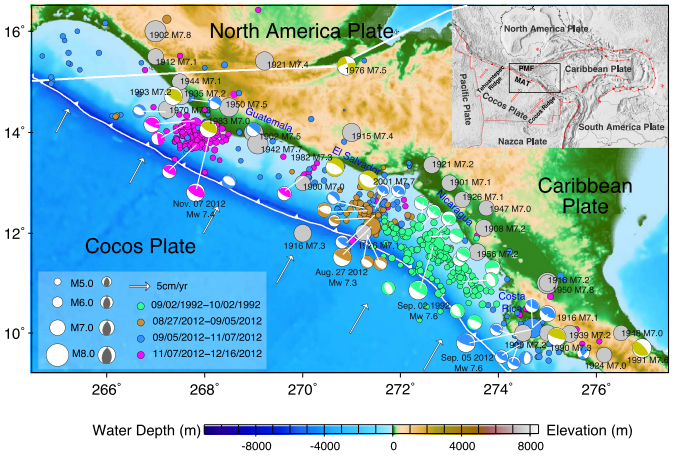

Fig. 1. Large earthquakes around the Middle American subduction zone from Costa Rica to Guatemala. Gray circles indicate epicenters of $M \geqslant 7.0$ events from 1900 to 1975 from PAGER-CAT (Allen et al., 2009). Focal mechanisms are global Centroid Moment Tensor (gCMT) solutions for $M \geqslant 7.0$ events from 1976 to 2012 (olive) plotted at the USGS/NEIC epicenters. Color-coded circles are epicenters for aftershock sequences of the September 2, 1992 Nicaragua (M_w 7.6) tsunami earthquake (green), the August 27, 2012 El Salvador (M_w 7.3) earthquake (brown), the September 5, 2012 Costa Rica (M_w 7.6) earthquake (blue), and the November 7, 2012 Guatemala (M_w 7.4) earthquake (magenta). Correspondingly colored gCMT mechanisms for these four sequences are shown. White curves indicate the Middle America Trench (MAT) boundary (barbed) between the Cocos Plate and Caribbean Plate, and the approximate North America and Caribbean plate boundary. Arrows indicate plate motion direction and rate relative to a fixed Caribbean plate computed using model NUVEL-1 (Argus and Gordon, 1991). The Cocos Plate subducts northeastward beneath the Caribbean Plate at 75 to 85 mm/yr with ~20–25% obliquity along Nicaragua, and at 65 to 75 mm/yr offshore of El Salvador and Guatemala with negligible obliquity. The inset map shows the regional plate tectonic setting. The red vectors indicate the plate motions relative to a fixed Caribbean Plate for model NUVEL-1. The relative motion between North America and Caribbean plates is left-lateral with rate of ~20 mm/yr across the Polochic–Motagua Fault zone (PMF).

CA plate along southern Costa Rica and/or pinning of the westernmost triangular region of the CA plate between the converging CO and NA plates near the triple junction (Franco et al., 2012; LaFemina et al., 2009). In contrast to the Mexican subduction zone to the northwest, where generally strong seismic coupling between the converging NA and CO plates is found, the upper CA plate is moving away from the MAT such that lower tectonic and seismic coupling may be expected. However, the inference of little megathrust coupling is complicated by the GPS sites being located far from the MAT, as well as by uncertainty in the locations and rupture characteristics of historical seismic events in the region.

Large subduction zone earthquakes do occur along the MAT (Fig. 1), including sources that produce destructive tsunami, like the 1902 Guatemala and 1992 Nicaragua tsunami earthquakes (Fernandez et al., 2000; Kanamori and Kikuchi, 1993), and there are an unusual number of outer-rise and down-dip normal faulting events along the arc (Supplemental Fig. S1). Casual inspection of the seismicity in Figs. 1 and S1 does not immediately suggest very weak seismic coupling, especially allowing for possible landward mislocation of some of the historical large events in the regions. As a result, there is substantial uncertainty regarding the potential for much larger underthrusting events in the region than have been documented in the seismological record.

Earthquake focal mechanism and seismic strain rate analyses (DeMets, 2001; Guzman-Speziale and Gomez-Gonzales, 2006; Harlow and White, 1985; McNally and Minster, 1981; White and Harlow, 1993; Pacheco et al., 1993) indicate that only ~10% to 20% of the CO–CA plate motion is seismically manifested in trench-perpendicular underthrusting events, so the cumulative seismic activity in Figs. 1 and S1 actually does fall far short of the plate motion convergence rate even allowing for uncertainty in older event locations and mechanisms. Despite this, numerous strike-slip events occur along the Middle America volcanic arc, as is typically observed for strain partitioning that accompanies oblique subduction in strongly-coupled regions (DeMets, 2001; Fitch, 1972; McCaffrey, 1992). It has been estimated that the strike-slip earthquake strain budget may match the geodetic rates, suggesting 80–100% seismic coupling of that boundary of the sliver (Correa-Mora et al., 2009).

In 2012, the megathrust between the CO and CA plate sliver experienced three large ruptures: the August 27, 2012 M_w 7.3 El Salvador, September 5, 2012 M_w 7.6 Costa Rica, and November 7, 2012 M_w 7.4 Guatemala earthquakes (Table S1). Together with the September 2, 1992 M_w 7.7 Nicaragua event (Table S1), these large thrust earthquakes shed light on the nature of the Middle America megathrust rupture processes in the context of the geodetic inferences of very weak plate boundary seismic coupling extending from Guatemala to northern Costa Rica. We analyze the rupture characteristics of the four large events and aftershock sequences for the three 2012 events (Fig. 1) to explore the nature of megathrust failure properties along the MAT.

2. Rupture process characteristics of large earthquakes

We first quantify the overall faulting parameters for the four large thrust events along the MAT. These are the largest events on the megathrust for which we have high quality observations, and they define the minimum degree of seismic coupling of the plate boundary.

2.1. W-phase inversion

Three-component W-phase signals in the 1.67–5.0 mHz passband were inverted for point-source moment tensors for the 1992 and 2012 events. Fig. S2 shows that the preferred solutions for: (a) the 1992 Nicaragua event with seismic moment of 4.1×10^{20} Nm (M_w 7.7), centroid time shift of 47.8 s, depth 15.5 km, and a best double-couple solution with strike 289.0°, dip 14.7°, and rake 65.3°; (b) the 2012 El Salvador event with seismic moment of 9.6×10^{19} Nm (M_w 7.3), centroid time shift of 23.0 s, depth 15.5 km, and a best double-couple solution with strike 284.4°, dip 17.2°, and rake 78.9°; (c) the 2012 Costa Rica event with seismic moment 3.3×10^{20} Nm (M_w 7.6), centroid time shift of 19.5 s, depth 30.5 km, and a best double-couple solution with strike 303.4°, dip 15.7°, and rake 94.2°; and (d) the 2012 Guatemala event with seismic moment of 1.2×10^{20} Nm (M_w 7.3), centroid time shift of 10.6 s, depth 23.5 km, and a best double-couple solution with strike 293.1°, dip 28.5°, and rake 77.8°. Examples of waveform fits for each case are shown in Supplemental Fig. S3. The estimates of depth and centroid time shift are similar to the centroid depths of 15 km, 12.0 km, 29.7 km, and 21.3 km, and centroid time shifts of 44.5 s, 20.1 s, 15.4 s and 9.6 s from the global Centroid Moment Tensor (gCMT) project (http://www.globalcmt.org/CMTsearch.html) for the 1992 Nicaragua and 2012 El Salvador, Costa Rica, and Guatemala events, respectively. Although their magnitudes are similar, the W-phase centroid time shift of the El Salvador event is ~3 times larger than for the Guatemala event, and about half that for the 1992 Nicaragua tsunami earthquake, whose overall source time function duration is ~100 s (Kanamori and Kikuchi, 1993). This indicates a relatively slow rupture process of the 2012 El Salvador earthquake.

2.2. Finite-fault rupture inversions

Finite-fault rupture models were developed using teleseismic P waves for all four large events. Fig. 2 summarizes the slip distribution models found from the P wave ground motions in the frequency band 0.005–0.9 Hz using the linear inversion procedure

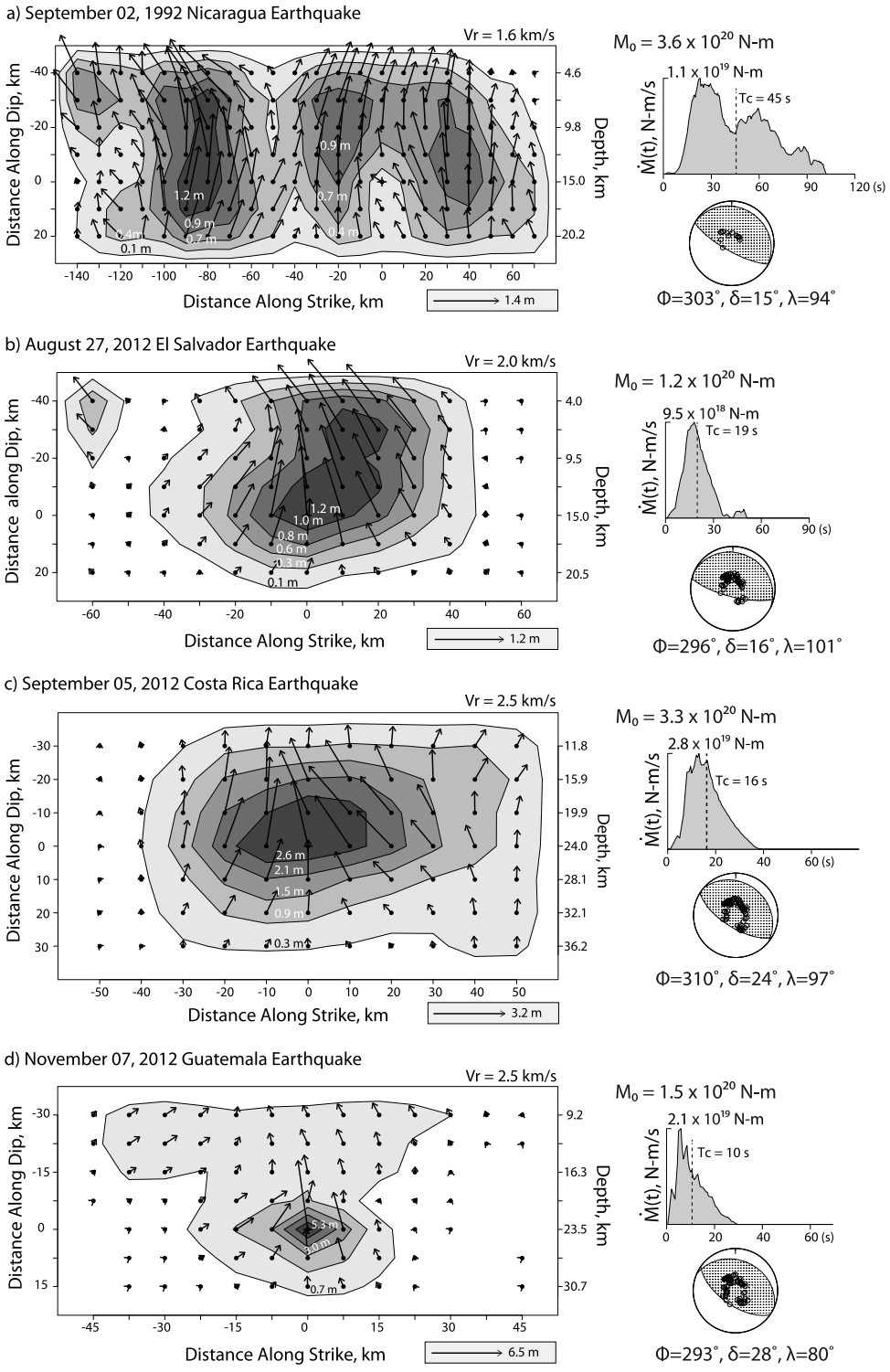

Fig. 2. Finite-fault slip models from teleseismic P wave inversion for (a) September 2, 1992 Nicaragua, (b) August 27, 2012 El Salvador, (c) September 5, 2012 Costa Rica and (d) November 7, 2012 Guatemala earthquakes. The slip distribution on the fault plane is shown for each case with the arrows indicating average rake of each subfault, and the slip magnitude being contoured. Peak slip is indicated for each model, along with the rupture expansion velocity, Vr. The moment-rate functions, seismic moments, centroid times (Tc), and average focal mechanisms are shown, with the lower hemisphere equal area projections indicating the positions sampled by teleseismic P waves used in the inversions. Observed and synthetic P wave comparisons are shown in supplementary Fig. S4.

of Kikuchi and Kanamori (1991). This inversion method assumes a constant rupture velocity for a fault geometry with specified strike and dip, allowing variable rake, and uses modest smoothing to stabilize the temporal and spatial moment distribution.

For the September 2, 1992 Nicaragua earthquake, 13 broadband P waves with 130 s duration signals were inverted (examples of waveform fits are shown in Supplemental Fig. S4a). We assumed a hypocenter depth of 15 km, 3 km water depth, a rupture velocity of 1.6 km/s, a strike of 303°, a shallow 15°-dipping fault plane extending from the MAT to about 23 km depth, and subfault source time functions parameterized by 4 overlapping 2 s rise-time triangles (total subfault duration of 10 s) with variable rake. These choices were guided by previous studies of the limited number of broadband teleseismic P waves, surface

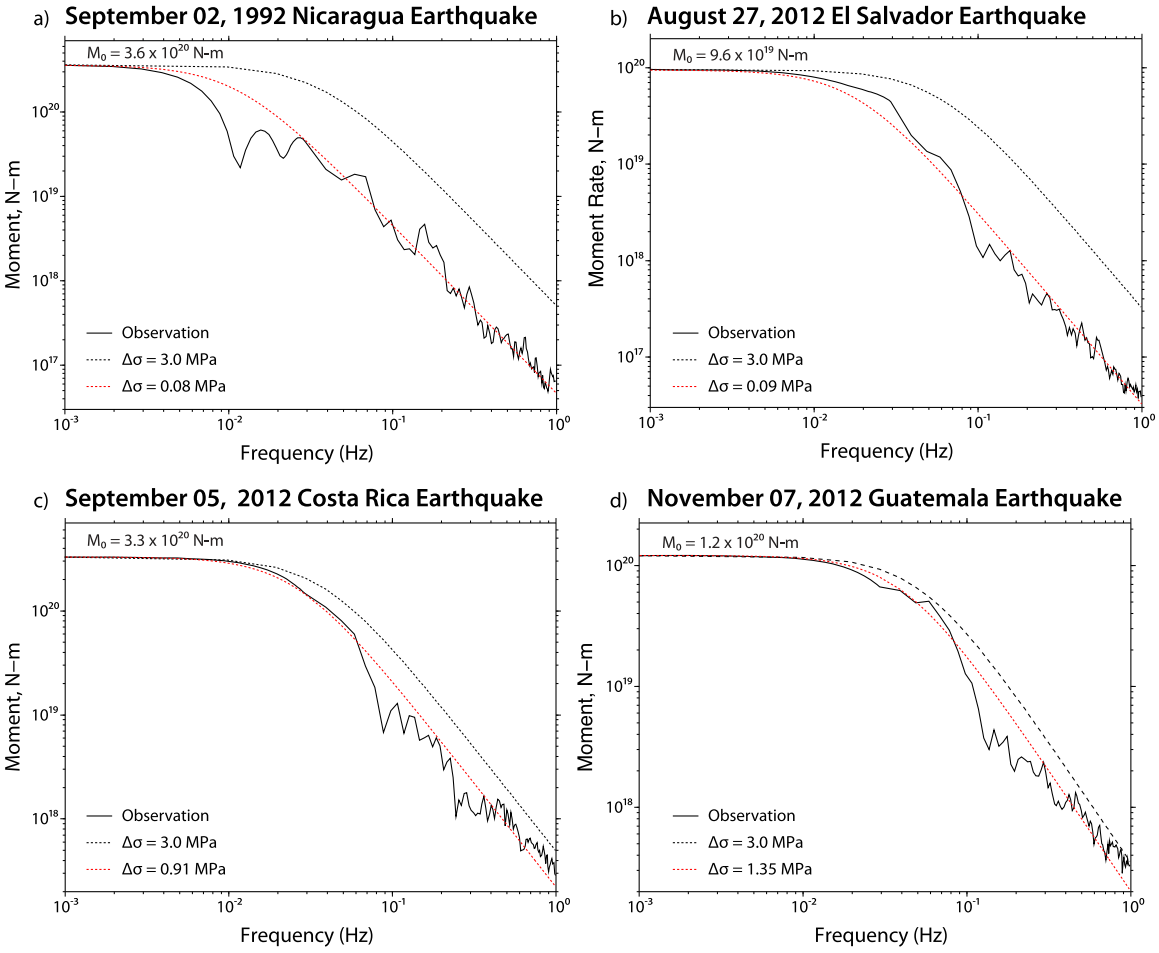

Fig. 3. The average source spectra for teleseismic P waves for the large thrust events in Middle America. In each panel, the black line indicates the observed spectra, estimated at frequencies less than ~0.05 Hz from the moment-rate function inverted from teleseismic P wave observations (Fig. 2) and at frequencies >~0.05 Hz from stacking of broadband teleseismic P wave spectra. The dashed lines are reference source spectra for an ω^{-2} model with 3 MPa stress parameter (black) and best fitting ω^{-2} models with different stress parameters (red), with fixed shear velocity, $\beta = 3.75$ km/s, and seismic moments given by the W-phase inversions (2012 El Salvador and 2012 Guatemala events) or P wave inversions (1992 Nicaragua and 2012 Costa Rica events).

waves and tsunami observations (e.g. Kanamori and Kikuchi, 1993; Imamura et al., 1993; Satake, 1994; Velasco et al., 1994).

The rupture model (Fig. 2a) has three slip concentrations; a ~60 km wide patch to the southeast (with peak slip ~1.4 m) and two smaller 30 km wide patches (with peak slip ~0.9 m) on either side of the hypocenter, with rupture extending from the trench to ~23 km deep. The slip model supports the slow asymmetric bilateral rupture model of Velasco et al. (1994). The seismic data do not provide strong constraints on the along-dip width of the rupture; narrower rupture models with width of 40 km extending to 10 km deep, as proposed from tsunami modeling by Satake (1994), can be reconciled with the data, as can wider models. The seismic moment of this model, 3.6×10^{20} Nm is compatible with the long-period estimates of 4.1×10^{20} Nm from W-phase inversion and 3.7×10^{20} Nm from long-period surface waves (Kanamori and Kikuchi, 1993) and estimates of 3.4×10^{20} Nm from the gCMT and from body wave inversions (Kikuchi and Kanamori, 1995). The 100 s duration of the source time function, with a centroid time of 45 s, is also consistent with earlier studies. Given the limited data available, the resolution of the model is lower than for the more recent events, but we believe this model captures first-order attributes of the rupture well.

For the August 27, 2012 El Salvador event we inverted 83 broadband P waves with 100 s durations for a fault geometry with strike 296° and dip 16°, again extending from the trench to about 23 km deep, and a hypocentral depth of 15 km. A rupture velocity of 2 km/s, was used, with little direct constraint on that choice. The subfault source time functions had six overlapping 2 s rise-time triangles spanning a 14 s long total duration. The resulting model (Fig. 2b) has a single large-slip patch, extending across the fault width and ~50 km along strike, with peak slip of ~1.2 m and total seismic moment of 1.2×10^{20} Nm (M_w 7.3), about 20% larger than the W-phase solution. The source time function has ~40 s duration with a centroid time of 19 s. Waveform comparisons are shown in Supplemental Fig. S4b. The waveforms are relatively simple and the source model has limited spatial resolution as a result. Using a deeper hypocenter gives a more compact slip distribution, but our model is compatible with the 12 km centroid depth of the gCMT solution.

For the Costa Rica and Guatemala events larger centroid depths are indicated by the gCMT and W-phase long-period solutions. We explored a range of source depths and dip angles guided by the regional slab geometry to find our preferred finite-faulting inversions of ~70 broadband teleseismic P signals in each case (examples of the waveform fits are shown in Figs. S4c and S4d). For the September 5, 2012 Costa Rica earthquake we settled on a hypocenter depth of 24 km and fault plane dip of 24° dip and strike of 310°, a rupture velocity of 2.5 km/s, and subfault source time functions with 4 overlapping 3 s rise-time triangles (total subfault duration of 15 s). The slip model in Fig. 3c has a large-slip patch with peak slip of ~3.2 m extending from 10–35 km in depth and ~80 km along strike, with a total seismic moment of

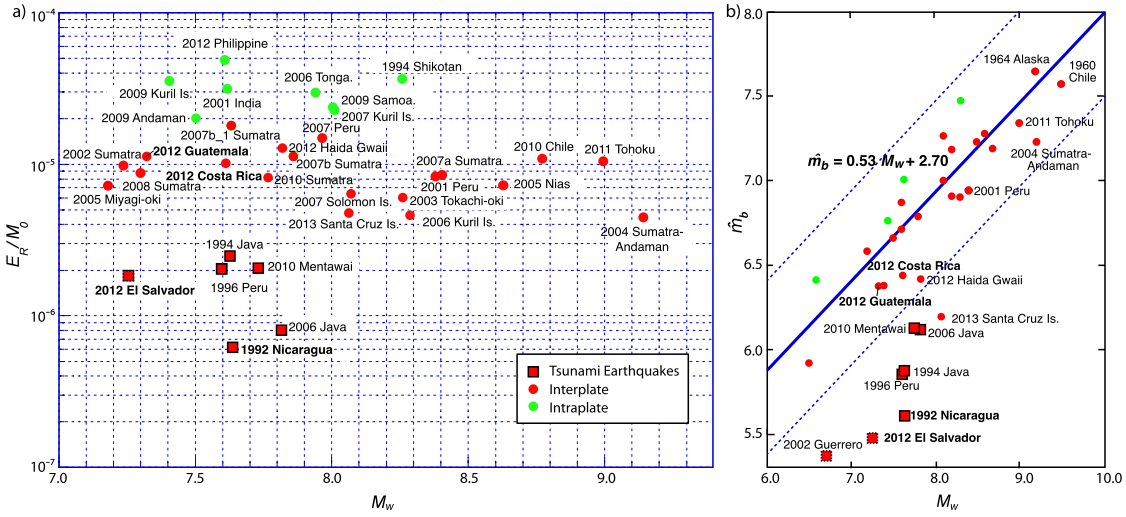

Fig. 4. (a) Estimates of seismic moment-scaled radiated seismic energy from teleseismic P wave ground velocity spectra and broadband source time functions from finite source inversions for recent large earthquakes. The 2012 El Salvador event has low moment-scaled energy typical of larger tsunami-earthquake ruptures. Note that the 2012 Costa Rica and 2012 Guatemala events have ~5–6 times higher seismic moment-scaled radiated energy. (b) Short-period $\hat{m}_b$ measurements for large earthquakes, plotted versus their seismic moment magnitudes. $\hat{m}_b$ is similar to conventional m_b, but uses the peak 1 s period amplitude over the full duration of the P waves rather than just the first few cycles of the waveforms, so it gives a better estimate of the overall ~1 s spectral level. Color-coded circles indicate interplate earthquakes (red) and intraplate earthquakes (green), and red squares with black outline indicate interplate tsunami earthquakes. The 2012 El Salvador earthquake has a similar value to the 1992 Nicaragua tsunami earthquake, but was too small to generate a large tsunami. The 2012 Costa Rica event and 2012 Guatemala event have $\hat{m}_b$ similar to typical interplate ruptures, although on the low end of the suite of observations. The blue line shows the $\hat{m}_b$ – seismic moment magnitude relationship obtained by Houston and Kanamori (1986).

3.3×10^{20} Nm (M_w 7.6) and centroid rupture time of 16 s. For the November 7, 2012 Guatemala earthquake, the hypocenter depth is 23.5 km, with dip of 28° and strike of 293°, a rupture velocity of 2.5 km/s and subfault source time functions comprised of 4 overlapping 1.5-s rise-time triangles (total subfault rupture durations of 7.5 s). A slip concentration with peak slip of 5.3 m, is found near the hypocenter, spread from 20–25 km in depth and ~20 km along strike. The centroid time is 10 s. Minor, poorly resolved slip extends up-dip to ~10 km depth, and the total seismic moment is 1.5×10^{20} Nm (M_w 7.4), about 20% higher than the W-phase estimate. The moment-rate functions for Costa Rica and Guatemala events have more pronounced jagged short-duration pulses than the shallower events, which may correspond to relative enrichment in high frequency radiation.

3. Short-period seismic wave radiation characteristics

We extend the rupture characterization of the four large thrust events to include their short-period seismic wave radiation, computing azimuthally-averaged P wave source spectra, seismic moment-scaled radiated energy, E_r/M_0, and ~1 s period P wave magnitudes measured over the full duration of the source radiation, $\hat{m}_b$ (Houston and Kanamori, 1986).

Broadband source spectra were obtained by combining the spectra of the moment-rate functions for the preferred finite-fault models in Fig. 2 for frequencies less than ~0.05 Hz with averages of radiation-pattern- and attenuation-corrected teleseismic broadband P wave spectra for frequencies from 0.05 to 1 Hz. Fig. 3 shows the resulting source spectra, along with reference source spectra for an ω^{-2} model with 3 MPa stress parameter (Brune, 1970). The spectra for the El Salvador and Guatemala events are normalized to the W-phase moment estimates because the P wave estimates appear about 20% high. The source spectra were fit with ω^{-2} models by varying the stress parameter and holding the shear velocity (β) fixed at 3.75 km/s. The best fitting models have low stress parameters of 0.08 and 0.09 MPa for the 1992 Nicaragua and 2012 El Salvador events, respectively, and more typical interplate stress parameters of 0.91 and 1.35 MPa for the 2012 Costa Rica and 2012 Guatemala events, respectively.

Total radiated seismic energy was estimated using the energy fraction computed for 0.05–1.0 Hz teleseismic P wave ground velocity spectra relative to the lower frequency energy content following the theory and method of Venkataraman and Kanamori (2004) and Rivera and Kanamori (2005). Large uncertainties are introduced by poor knowledge of the average P and S wave velocities around the sources, as well as limited data bandwidth and uncertainty in propagation corrections, particularly attenuation. The inclusion of the low-frequency energy contribution is essential for the 1992 Nicaragua and 2012 El Salvador events, for which the spectra are depleted in short-period energy. The total radiated energy estimates are 2.24×10^{14} J, 1.67×10^{14} J, 3.36×10^{15} J and 1.37×10^{15} J for the Nicaragua, El Salvador, Costa Rica and Guatemala events, respectively. The USGS estimates of energy magnitude, M_e, are 7.4 for the El Salvador and 7.9 for the Costa Rica and Guatemala events.

Fig. 4a shows the seismic moment-scaled radiated seismic energy for the large Middle America subduction zone events along with values for other interplate and intraplate events. Known tsunami earthquakes are highlighted. The 1992 Nicaragua event has the lowest E_r/M_0, 6.22×10^{-7}, among all events in Fig. 4a, while the 2012 El Salvador event also has a low E_r/M_0, 1.85×10^{-6}, similar to tsunami earthquakes. The 2012 Costa Rica and 2012 Guatemala events have E_r/M_0 ratios, 1.02×10^{-5} and 1.13×10^{-5}, respectively, similar to interplate events in other subduction regions.

The relative short-period seismic wave radiation levels are also measured by the $\hat{m}_b$ values, which are 5.6, 5.5, 6.4 and 6.4 for the Nicaragua, El Salvador, Costa Rica and Guatemala events, respectively. These values generally track the USGS m_b values given in Table S1, although the value for the 1992 Nicaragua event is relatively increased by using the full P wave signal window to measure the 1 Hz signal level. Fig. 4b shows that the magnitude difference between M_w and $\hat{m}_b$ is ~2 for the 1992 Nicaragua and 2012 El Salvador events and 0.8 for the 2012 Costa Rica and Guatemala events.

To further establish the radiation characteristics, we compare teleseismic and regional P wave signals for the 2012 El Salvador and 2012 Costa Rica earthquakes at common stations. Fig. S5

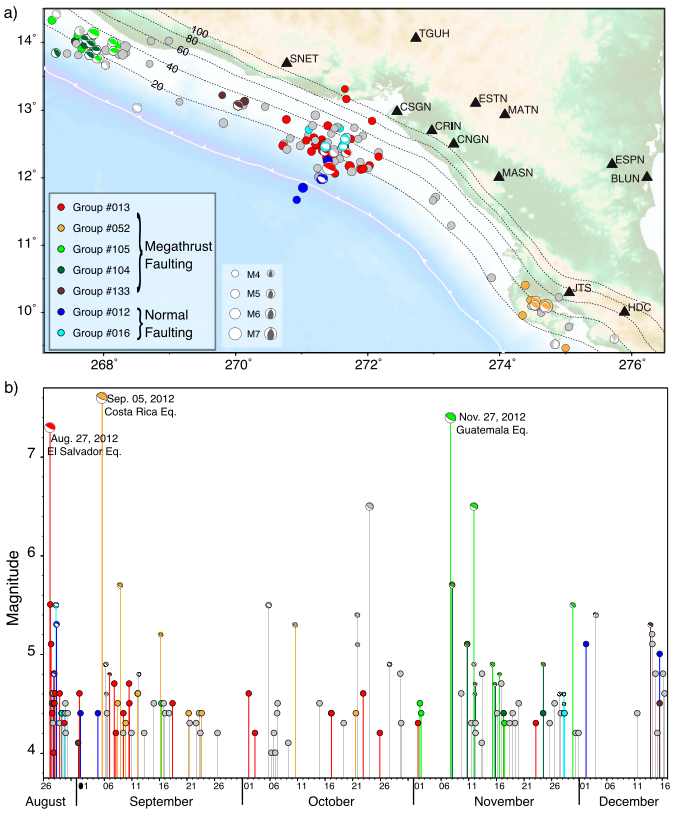

Fig. 5. (a) Locations of $m_b \geqslant 4.0$ events in the aftershock sequences for the three 2012 mainshocks from the USGS/NEIC catalog. Color-coded circles indicate similarity of three-component waveforms at station TGUH (triangle) to reference underthrusting events 013 (red) and 133 (dark brown) offshore of El Salvador, 052 (tan) under Costa Rica, 104 (dark green) and 105 (green) offshore of Guatemala, and offshore El Salvador normal faulting events 012 (blue) and 016 (light blue). The reference event focal mechanisms are from gCMT. Grey circles are events with no classification of mechanism. Waveforms are shown in Fig. S6. White barbed curve indicates the position of the trench. Triangles indicate stations used for spectral analysis. The white barded curve indicates the position of the MAT, and dash lines show the slab depth contours in km. (b) Time series for the aftershock sequence color-coded as in the map.

shows that the teleseismic P waves are not dramatically different waveforms, but the first arrivals do have more impulsive character for the Costa Rica event. The regional P wave ground velocity recordings at comparable propagation distances have signal amplitude ratios for frequencies >1 Hz relative to <0.1 Hz that are a factor of 3.6–5.6 larger for the Costa Rica event than for the El Salvador event, consistent with the factor of 5.5 higher seismic moment-scaled radiated energy (Fig. S5).

4. Aftershock sequence characterization

Substantial aftershock sequences (Fig. 1) followed the three large 2012 thrust earthquakes, with 141 events with $m_b \geqslant 4.0$ including the mainshocks (Table S2) being well recorded by regional broadband station TGUH and several Nicaragua broadband network (NU) stations (Fig. 5). 24 of the aftershocks have gCMT solutions with normal faulting or thrust fault mechanisms, as shown in Fig. 5. We are particularly interested to identify events with faulting mechanisms similar to the mainshocks which are likely to be on the plate interface. The main objective is to evaluate the seismic radiation efficiency for small events to see whether there are similarities to the large event characteristics.

We used cross-correlations of three-component broadband recordings at TGUH filtered in the passband of 0.01–0.05 Hz for the vertical components and 0.02–0.05 Hz for horizontal components to identify similar waveform clusters for nearby events. We use template waveforms from events with known gCMT focal mechanisms (Fig. S6). There are 28, 10 and 10 events with focal mechanisms similar to the 2012 El Salvador, Costa Rica and Guatemala mainshocks, respectively. 4 events have waveforms similar to two near-trench intraplate normal faulting events (012 and 017), and 7 events have waveforms similar to forearc normal faulting event 016. 7 events have similar waveforms to thrust event 104, which has distinct waveforms from the 2012 Guatemala event, and 3 events with similar waveforms to offshore thrust event 133 between Guatemala and El Salvador. Other events are too small or have focal mechanisms distinct from the nearby template events. The activation of normal faulting by the 2012 El Salvador event is similar to other large tsunami earthquakes, possibly indicating relatively complete stress release on the megathrust and/or slip extending up to the trench. Fig. 5 indicates the spatial and temporal distribution of the clusters of similar mechanism events, along with the distribution of unclassified events.

Having identified events with similar focal mechanisms in close spatial proximity, we use the regional broadband waveforms to estimate basic source spectral characteristics. This involved modeling of spectral ratios of common component recordings at the same station for events with similar mechanisms separated in location by $\leqslant$50 km. The data distribution allows us to examine spectral differences among the thrust populations along the megathrust and the difference between the thrust and normal faulting populations along El Salvador. Time windows of 10 s before to 150 s after the manually picked P arrivals in the regional broadband recordings from TGUH and the NU network stations shown in Fig. 5 are used. The most reliable spectral ratios with substantial bandwidth are baseline adjusted in the 0.1–0.2 Hz spectral band relative to the vertical component ratios for TGUH, and average spectral ratios computed from 3 to 10 individual ratios. These averaged spectral ratios were then modeled, with propagation and site effects ideally being canceled out, isolating the source spectrum differences.

For the spectral ratio modeling we assumed the spectral shape of the ω^{-2} source model, parameterized by a moment level and a corner frequency parameter. We varied the seismic moment of the denominator event relative to specified gCMT seismic moment for the numerator event, along with the corner frequencies of both numerator and denominator events. The procedure is most robust for event pairs with large differences in corner frequency and seismic moment, and good signal-to-noise ratio over substantial bandwidth. Examples of the spectral ratio averaging and modeling are shown in Fig. S7. The ratios have increasing variance at higher frequencies, and not all of the spectral ratios tightly define the smaller event's corner frequency, but this mainly affects the smallest events. The spectral ratios are not reliable above 3 Hz where the ratios abruptly rise or drop off, so modeling was constrained to frequencies $\leqslant$3 Hz. The parameter estimation was performed by grid searching over the 3 adjustable spectral parameters rather than by inversion. In general the spectral ratios are modeled adequately with the simple point-source parameterization although some event pairs have spectral ratio complexity not represented by the simple sources. Our signal windows capture essentially the full regional waveform, so body and surface waves are included. This allows us to have substantial bandwidth and avoids challenges of phase windowing, but does mean that our source spectral characterizations are gross measures of the seismic radiation, not individual phase spectra.

Fig. 6 shows that the corner frequency estimates, normalized relative to a reference constant stress parameter (3 MPa) ω^{-2} source model with shear velocity 3.75 km/s, exhibit systematic spatial distributions. The normalized corner frequencies for thrust faulting events tend to increase from anomalously low values closer to the MAT to higher values, scattered around the reference

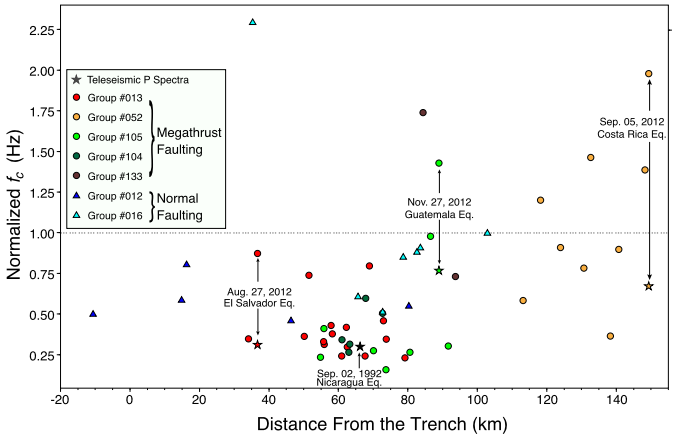

Fig. 6. Corner frequencies, normalized by 3 MPa ω^{-2} source model with shear velocity 3.75 km/s, from fitting the spectral ratios of similar focal mechanism events for likely interplate thrust events (circles) and intraplate normal faulting events offshore El Salvador (triangles), plotted as a function of perpendicular distance from the trench to the USGS/NEIC source locations. The stars show the normalized corner frequencies from fitting teleseismic P wave spectra (Fig. 3). Note the trend of increasing normalized corner frequencies for (likely) interplate thrust events from anomalously low values closer to the trench to higher values at greater distances, and the high normalized corner frequencies offshore Costa Rica. Intraplate normal faulting events tend to have higher normalized corner frequencies than interplate earthquakes offshore El Salvador. Examples of the spectral ratio fitting are shown in supplementary Fig. S7.

model further down-dip. This trend may involve along-strike variation as well, given that the deeper events are mainly near Costa Rica, with many shallower events being along El Salvador. Intraplate normal faulting events tend to have higher normalized corner frequencies than interplate earthquakes along El Salvador. The source parameter estimates from the regional wave spectra for the three large thrust events have higher normalized corner frequencies from regional data than inferred from the teleseismic P wave spectra (Fig. 3), although the relative shifts are similar. This may due to spectral superposition of multiple arrivals and source-finiteness effects in the full regional waveform spectra (Molnar et al., 1973; Savage, 1972) relative to the single phase measures given by the teleseismic data.

While there is a lot of scatter and the approximate uncertainty for each estimate is ±30%, the basic pattern of difference in spectral character between the El Salvador (red) and Guatemala (green) events relative to the Costa Rica (tan) events appears reliable, as does the tendency for intraplate normal faulting to have higher normalized corner frequencies along El Salvador. Allmann and Shearer (2009) find that the Central America region has very low stress drop measures for thrust events along the Cocos subduction zone, including along Mexico, Guatemala and Nicaragua, whereas intraplate events had more typical stress drop estimates. The basic trend seen in Fig. 6 is also compatible with the results of Convers and Newman (2011) who analyzed radiated seismic energy for 53 large thrust events along the MAT with $M_w \geqslant 6.7$. They found that on average the $\log_{10}$ (radiated energy/seismic moment) discriminant value along the MAT (−5.15) is lower than the global average value (−4.74) for thrust events, indicating energy deficiency by about a factor of 3. All of their events off of Nicaragua and Costa Rica were energy deficient, with some events off of Chiapas, Mexico and Guatemala having higher energy. They observed a slight trend of increasing energy with depth, but there is again a lot of scatter, so it is difficult to distinguish from lateral variations. Overall, the tendency for interplate events on the megathrust along the MAT to have lower corner frequencies and lower radiated energy appears to hold for events ranging in size from $m_b \sim 4$ to $M_w \sim 7.6$, suggesting that this is related to the interplate frictional properties, not just unusual rupture of the largest events.

5. Discussion

The nature of interplate coupling along the Middle America megathrust can now be considered in the light of joint seismic and geodetic observations. The large thrust events of 2012 provide a significantly expanded sampling of well-quantified seismological observations of earthquake ruptures to supplement the extensive geodetic data sets acquired in the past few decades. We update and refine the seismic strain rate estimates from previous studies by focusing exclusively on shallow-dipping thrust earthquakes in the gCMT catalog since 1976, which is fairly complete down to about M_w 5.0. We only consider events with centroid depths less than 40 km along the plate boundary from northern Guatemala to Nicoya, Costa Rica as shown in Fig. 7a. There is some depth uncertainty in the gCMT catalog, and some events with overestimated source depths or deeper coupled portions of the plate boundary may be excluded, but the number of such events is small and their inclusion would not change the basic result we find here. The cumulative seismic moment for these events is $\sim 1.01 \times 10^{21}$ Nm, of which 9.54×10^{20} Nm is from the 1992 Nicaragua, 2012 El Salvador, 2012 Costa Rica and 2012 Guatemala events. We estimate a seismogenic megathrust length of 1300 km, width of 100 km, and area of $\sim 1.3 \times 10^5$ km^2. The CO–CA convergence rate is ~72 mm/yr along Guatemala to ~85 mm/yr along Nicoya (DeMets, 2001), so we assume an average value of 78 mm/yr for the region. The 37-year interval seismic moment rate to tectonic convergence rate ratio is ~6.7%, assuming an average rigidity of 40 GPa along the megathrust. This estimate is comparable with the seismic coupling estimates of ~3%–20% along the MAT by Pacheco et al. (1993) and ~10% from 1976–2003 by Guzman-Speziale and Gomez-Gonzalez (2006). The 37-year period is certainly too short for robust seismic coupling estimation given the regional estimate of recurrence time of ~50–70 yrs for $M7+$ events (Nishenko, 1991), but it is very difficult to justify inclusion of historical events with uncertain locations and focal mechanisms, especially given the well-documented and extensive occurrence of intraplate normal faulting and strike-slip faulting in the nearshore and offshore regions. We note that the measure of cumulative moment release over a fixed interval of time is not the ideal measure of seismic coupling, which would use time intervals between repeated ruptures of the same fault subregions, but we lack information about slip in any prior large ruptures in the regions of the recent events so this is all that can be done.

We summarize the extensive GPS observations and inferences that have accumulated and been published over last two decades, plotting them relative to a fixed Caribbean plate in Fig. 7b. The inferred relative motions between NA, CO, CA and the forearc sliver, as well as the internal deformation are noted. The NA/CA motion decreases from ~20 mm/yr in eastern Guatemala along the Polochic–Motagua fault zone down to a few millimeters per year in western Guatemala. There is ~5–10 mm/yr E–W extension within the CA plate in northwestern Honduras adjacent to Guatemala and El Salvador, where shallow normal faulting events have occurred (Fig. 7a) (Franco et al., 2012; Lyon-Caen et al., 2006). The geodetic studies consistently indicate low or no coupling on the deeper portion of the megathrust below the forearc sliver, which is translating at ~10–16 mm/yr toward the NA–CO–CA triple junction in the CA reference frame. Given that the CA is moving away from the subduction zone, the relative motion of the sliver can be viewed as the forearc being left behind the retreating CA. 85–100% seismic coupling is estimated from strike-slip events along the volcanic arc on the northeast boundary of the sliver (Fig. 7a) (Franco et al., 2012). Two patches with ~10% and ~25–50% locking near El Salvador and Costa Rica, respectively, are suggested by Correa-Mora et al. (2009), with less than 2% on average over the entire megathrust along the sliver. Estimates of from 5 to 100% localized coupling

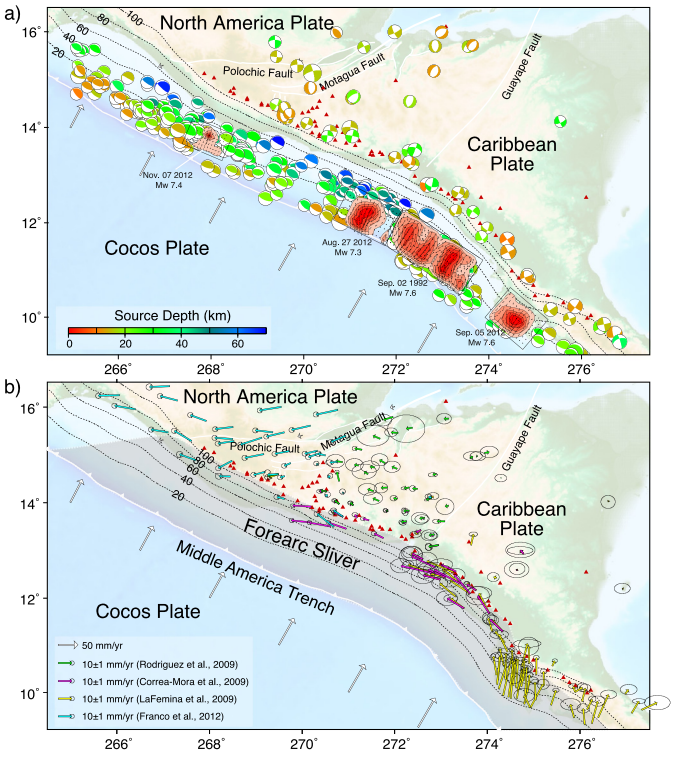

Fig. 7. (a) Map of gCMT focal mechanisms from 1976 to 2013 for interplate earthquakes on the MAT megathrust, strike-slip earthquakes along the volcanic arcs and the Polochic–Motagua faults, and shallow normal faulting events in the Caribbean Plate. Fault slip models for the 1992 Nicaragua, 2012 El Salvador, 2012 Costa Rica, and 2012 Guatemala earthquakes from finite-fault inversions (Fig. 2) are also shown. (b) Summary of the GPS velocity field measurements from four recent studies (Rodriguez et al., 2009; LaFemina et al., 2009; Correa-Mora et al., 2009; Franco et al., 2012) in the fixed Caribbean Plate reference frame. The white barbed curve indicates the position of the MAT, and dashed lines indicate 20-km increment slab depth contours. The forearc sliver that is undergoing boundary-parallel motion is shaded.

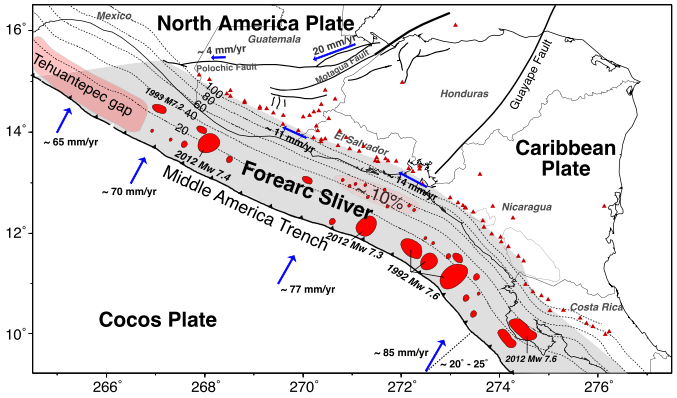

Fig. 8. Map showing plate and forearc motions relative to a fixed Caribbean Plate (blue) and schematic seismic asperities (red patches) that had/have high seismic coupling as inferred from slip models for large interplate thrusting events. The pale pink region offshore of El Salvador at depths from 30–60 km is inferred to have ~10% locking inverted from geodetic data (Correa-Mora et al., 2009). The Tehuantepec gap lacks any recorded large earthquake activity, but has been inferred to have about 60% locking based on geodetic observations (Franco et al., 2012).

over different scale lengths for the shallow megathrust along the sliver extending to about 20 km depth have been proposed in various studies (LaFemina et al., 2009; Rodriguez et al., 2009; Franco et al., 2012). Relatively strong locking of ~60% near the triple junction has been suggested, although part of this region is the Tehuantepec seismic gap, where no large historical earthquake activity has been recorded. These geodetic coupling estimates are summarized in Fig. S8.

Considering the seismic activity along the Middle America megathrust in the context of the cumulative moment estimate and the geodetic observations, we provide a schematic map (Fig. 8) that indicates generally low coupling on the megathrust below the forearc sliver, with localized asperities that had/have high seismic coupling inferred from the slip models and focal mechanisms of interplate thrusting events. This characterization is now much better defined as a result of our quantification of the three recent large earthquakes along the MAT. The region along Nicoya, Costa Rica has repeatedly experienced large interplate thrust events, suggesting a high-percentage of strong coupling, and this is consistent with the geodetic estimates of substantial areas of 100% locking prior to the 2012 event. Offshore of Nicaragua and El Salvador, the larger asperities appear to be located at depths from the trench to about 20 km deep, with patchy areas of ~40 km length scale, surrounded by weaker coupling. Failure of either several or individual patches led to the 1992 Nicaragua and 2012 El Salvador earthquakes with depleted short-period seismic radiation, low rupture velocity and tsunami-earthquake characteristics. Many of the smaller interplate events in this region appear to have anomalously low corner frequencies. Presence of subducted sediments on the megathrust may account for the low rupture velocities and weak short-period radiation during failure of the shallow megathrusts (e.g., Kanamori and Kikuchi, 1993; Polet and Kanamori, 2000). Intermediate size asperities exist on the megathrust at somewhat deeper depths along this region, giving rise to a few moderate size thrusting aftershocks and events like the October 9, 2004 M_w 6.9 event located down-dip of the 1992 Nicaragua event. Offshore of Guatemala and Chiapas, Mexico, localized asperity failures gave rise to the November 7, 2012 M_w 7.4 event and the September 10, 1993 M_w 7.2 event to the north, with normal radiation characteristics.

There is a large segment between El Salvador and Guatemala without a recent large event; it is hard to preclude isolated events like the 2012 events occurring in this region. However, the absence of upper plate strain in the convergence direction along the sliver from Nicaragua to Guatemala strongly suggests the patchy asperity distribution in Fig. 8 is about the upper limit of the seismically strongly-coupled portion of the megathrust in terms of what can be reconciled with the recent geodetic history. At face value, this appears to reduce the likelihood of a great earthquake rupturing along this boundary. There are several caveats to this interpretation: the 1992 Nicaragua event itself appears to involve a sequence of asperities failing in a single rupture, enhancing the tsunami excitation greatly relative to a single asperity failure like the 2012 El Salvador event. A cascade of multiple asperities failing along the megathrust, perhaps following rupture of one particularly large one, could give rise to a great rupture even without requiring uniform strong coupling. The relative timing of the three 2012 earthquakes and the overlap of their aftershock sequences indicates the potential for synchronization of proximity to failure along the arc. There is also a fundamental question about time-varying coupling; the shallow megathrust off of the Nicaragua event may have unusually slow healing and accumulation of upper plate strain due to the shallow frictional properties of that source region. These considerations make it difficult to rule out great events entirely.

6. Conclusions

Motivated by recent geodetic findings of little strain accumulation in the upper Caribbean plate along the Middle America subduction zone, we analyzed the seismological rupture characteristics of an unusual suite of three large thrust earthquakes that occurred in 2012, along with the 1992 Nicaragua tsunami earthquake.

A relatively long source duration, low seismic moment-scaled radiated energy, and depleted short-period seismic source spectrum is found for the 2012 El Salvador event, similar to the 1992 Nicaragua tsunami event which ruptured the adjacent shallow portion of the plate boundary. The 2012 El Salvador event was too small to generate a large tsunami but has attributes shared with other recent tsunami earthquakes. It seems quite plausible that other tsunami earthquakes can occur along the shallow megathrust extending from Guatemala to Nicaragua. Large 2012 ruptures along Costa Rica and Guatemala occur at greater depth on the megathrust and have more typical seismic moment-scaled radiated energy and source spectra. Underthrusting aftershocks of the El Salvador and Guatemala events have anomalously low relative corner frequencies, whereas deeper aftershocks of the Costa Rica event appear to be rather typical. This suggests that both large and small events are influenced by depth- or laterally-varying frictional properties, with events closer to the trench having lower than typical corner frequencies. The slip distributions, radiated energy and spectral variations suggest a patchy distribution of seismic coupling along the shallow megathrust, with cumulative seismic moment release over the past 37 years accounting for less than 10% of the plate motion budget. This is generally consistent with the geodetic inferences of weak interplate coupling and trench-parallel transport of a forearc sliver with little trench-perpendicular strain accumulation in the upper plate. While the potential for a great earthquake along the boundary may appear to be low given the inferred weak coupling, seismic hazard along the arc remains high due to the very seismogenic strike-slip system accommodating the sliver motions and the presence of large intraplate normal faulting in the slab just off the coast, along with upper plate deformation in the westernmost portion of the Caribbean plate. The possibility of a multi-asperity rupture growing into a great event along the arc cannot be ruled out, nor can concern about time-varying plate coupling, given the short observational history.

Acknowledgements

This work made use of GMT and SAC software. We appreciate comments from two anonymous reviewers and editor Peter Shearer. The IRIS DMS data center was used to access the seismic data from Global Seismic Network and Federation of Digital Seismic Network stations. This work was supported by NSF grant EAR0635570 (T.L.).

Appendix A. Supplementary material

Supplementary material related to this article can be found online at http://dx.doi.org/10.1016/j.epsl.2013.08.042.

References

Allen, T.I., Marano, K.D., Earle, P.S., Wald, D.J., 2009. PAGER-CAT: A composite earthquake catalog for calibrating global fatality models. Seismol. Res. Lett. 80, 57–62, http://dx.doi.org/10.1785/gssrl.80.1.57.

Allmann, B.B., Shearer, P.M., 2009. Global variations of stress drop for moderate to large earthquakes. J. Geophys. Res. 114, http://dx.doi.org/10.1029/2009JB005821.

Alvarado, D., DeMets, C., Tikoff, B., Hernández, D., Wawrzyniec, T.F., Pullinger, C., Mattioli, G., Turner, H.L., Rodriguez, M., Correa-Mora, F., 2011. Forearc motion and deformation between El Salvador and Nicaragua: GPS, seismic, structural, and paleomagnetic observations. Lithosphere 3 (1), 3–21, http://dx.doi.org/10.1130/L108.1.

Alvarez-Gomez, J.A., Meijer, P.T., Martínez-Díaz, J.J., Capote, R., 2008. Constraints from finite element modeling on the active tectonics of northern Central America and the Middle America Trench. Tectonics 27, http://dx.doi.org/10.1029/2007TC002162.

Argus, D.F., Gordon, R.G., 1991. No-net-rotation model of current plate velocities incorporating plate motion model NUVEL-1. Geophys. Res. Lett. 18 (11), 2039–2042.

Brune, J.N., 1970. Tectonic stress and the spectra of seismic shear waves from earthquakes. J. Geophys. Res. 75 (26), 4997–5009.

Convers, J.A., Newman, A.V., 2011. Global evaluation of large earthquake energy from 1997 through mid-2010. J. Geophys. Res. 116, http://dx.doi.org/10.1029/2010JB007928. B08304.

Correa-Mora, F., DeMets, C., Alvarado, D., Turner, H.L., Mattioli, G., Hernandez, D., Pullinger, C., Rodriguez, M., Tenorio, C., 2009. Evidence for weak coupling of the Cocos plate subduction interface and strong coupling of the volcanic arc faults from modeling of GPS data: El Salvador and Nicaragua. Geophys. J. Int. 179 (3), 1279–1291.

DeMets, C., 2001. A new estimate for present-day Cocos–Caribbean plate motion: Implications for slip along the Central American volcanic arc. Geophys. Res. Lett. 28 (21), 4043–4046.

Fernandez, M., Molina, E., Havskov, J., Atakan, K., 2000. Tsunamis and tsunami hazards in Central America. Nat. Hazards 22 (2), 91–116.

Fitch, T.J., 1972. Plate convergence, transcurrent faults, and internal deformation adjacent to southeast Asia and the western Pacific. J. Geophys. Res. 77 (23), 4432–4460.

Franco, A., Lasserre, C., Lyon-Caen, H., Kostoglodov, V., Molina, E., Guzman-Speziale, M., Monterosso, D., Robles, V., Figueroa, C., Amaya, W., Barrier, E., Chiquin, L., Moran, S., Flores, O., Romero, J., Santiago, J.A., Manea, M., Manea, V.C., 2012. Fault kinematics in northern Central America and coupling along the subduction interface of the Cocos Plate, from GPS data in Chiapas (Mexico), Guatemala and El Salvador. Geophys. J. Int. 189, 1223–1236.

Guzmán-Speziale, M., Gómez-González, J.M., 2006. Seismic strain rate along the Middle America Trench reveals significant differences between Cocos–North America and Cocos–Caribbean convergence. Geophys. J. Int. 166 (1), 179–185.

Harlow, D.H., White, R.A., 1985. Shallow earthquakes along the volcanic chain in Central America: Evidence for oblique subduction. Earthq. Notes 55 (1), 28.

Houston, H., Kanamori, H., 1986. Source spectra of great earthquakes: Teleseismic constraints on rupture process and strong motion. Bull. Seismol. Soc. Am. 76 (1), 19–42.

Imamura, F., Shuto, N., Ide, S., Yoshida, Y., Abe, K., 1993. Estimate of the tsunami source of the 1992 Nicaraguan earthquake from tsunami data. Geophys. Res. Lett. 20 (14), 1515–1518.

Kanamori, H., Kikuchi, M., 1993. The 1992 Nicaragua earthquake: A slow tsunami earthquake associated with subducted sediments. Nature 361, 714–716.

Kikuchi, M., Kanamori, H., 1991. Inversion of complex body waves—III. Bull. Seismol. Soc. Am. 81 (6), 2335–2350.

Kikuchi, M., Kanamori, H., 1995. Source characteristics of the 1992 Nicaragua tsunami earthquake inferred from teleseismic body waves. Pure Appl. Geophys. 144 (3–4), 441–453.

LaFemina, P., Dixon, T.H., Govers, R., Norabuena, E., Turner, H., Saballos, A., Mattioli, G., Protti, M., Strauch, W., 2009. Fore-arc motion and Cocos Ridge collision in Central America. Geochem. Geophys. Geosyst. 10 (5).

Lyon-Caen, H., Barrier, E., Lasserre, C., Franco, A., Arzu, I., Chiquin, L., Chiquin, M., Duquesnoy, T., Flores, O., Galicia, O., Luna, J., Molina, E., Porras, O., Requena, J., Robles, V., Romero, J., Wolf, R., 2006. Kinematics of the North America–Caribbean–Cocos plates in Central America from new GPS measurements across the Polochic–Motagua fault system. Geophys. Res. Lett. 33, http://dx.doi.org/10.1029/2006GL027696.

McCaffrey, R., 1992. Oblique plate convergence, slip vectors, and forearc deformation. J. Geophys. Res. 97 (B6), 8905–8915.

McNally, K.C., Minster, J.B., 1981. Nonuniform seismic slip rates along the Middle America Trench. J. Geophys. Res. 86 (B6), 4949–4959.

Molnar, P., Tucker, B.E., Brune, J.N., 1973. Corner frequencies of P and S waves and models of earthquake sources. Bull. Seismol. Soc. Am. 63 (6–1), 2091–2104.

Nishenko, S.P., 1991. Circum-Pacific seismic potential – 1989–1999. Pure Appl. Geophys. 135 (2), 169–259.

Pacheco, J.F., Sykes, L.R., Scholz, C.H., 1993. Nature of seismic coupling along simple plate boundaries of the subduction type. J. Geophys. Res. 98 (B8), 14133–14159.

Polet, J., Kanamori, H., 2000. Shallow subduction zone earthquakes and their tsunamigenic potential. Geophys. J. Int. 142, 684–702.

Rivera, L., Kanamori, H., 2005. Representations of the radiated energy in earthquakes. Geophys. J. Int. 162 (1), 148–155.

Rodriguez, M., DeMets, C., Rogers, R., Tenorio, C., Hernandez, D., 2009. A GPS and modelling study of deformation in northern Central America. Geophys. J. Int. 178 (3), 1733–1754.

Satake, K., 1994. Mechanism of the 1992 Nicaragua tsunami earthquake. Geophys. Res. Lett. 21 (23), 2519–2522.

Savage, J.C., 1972. Relation of corner frequency to fault dimensions. J. Geophys. Res. 77 (20), 3788–3795.

Turner, H.L. III, LaFemina, P., Saballos, A., Mattioli, G.S., Jansma, P.E., Dixon, T., 2007. Kinematics of the Nicaraguan forearc from GPS geodesy. Geophys. Res. Lett. 34, http://dx.doi.org/10.1029/2006GL027586. L02302.

Velasco, A.A., Ammon, C.J., Lay, T., Zhang, J., 1994. Imaging a slow bilateral rupture with broadband seismic waves: The September 2, 1992 Nicaraguan tsunami earthquake. Geophys. Res. Lett. 21, 2629–2632.

Venkataraman, A., Kanamori, H., 2004. Observational constraints on the fracture energy of subduction zone earthquakes. J. Geophys. Res. 109 (B5), http://dx.doi.org/10.1029/2003JB002549.

White, R.A., Harlow, D.H., 1993. Destructive upper-crustal earthquakes of Central America since 1900. Bull. Seismol. Soc. Am. 83 (4), 1115–1142.

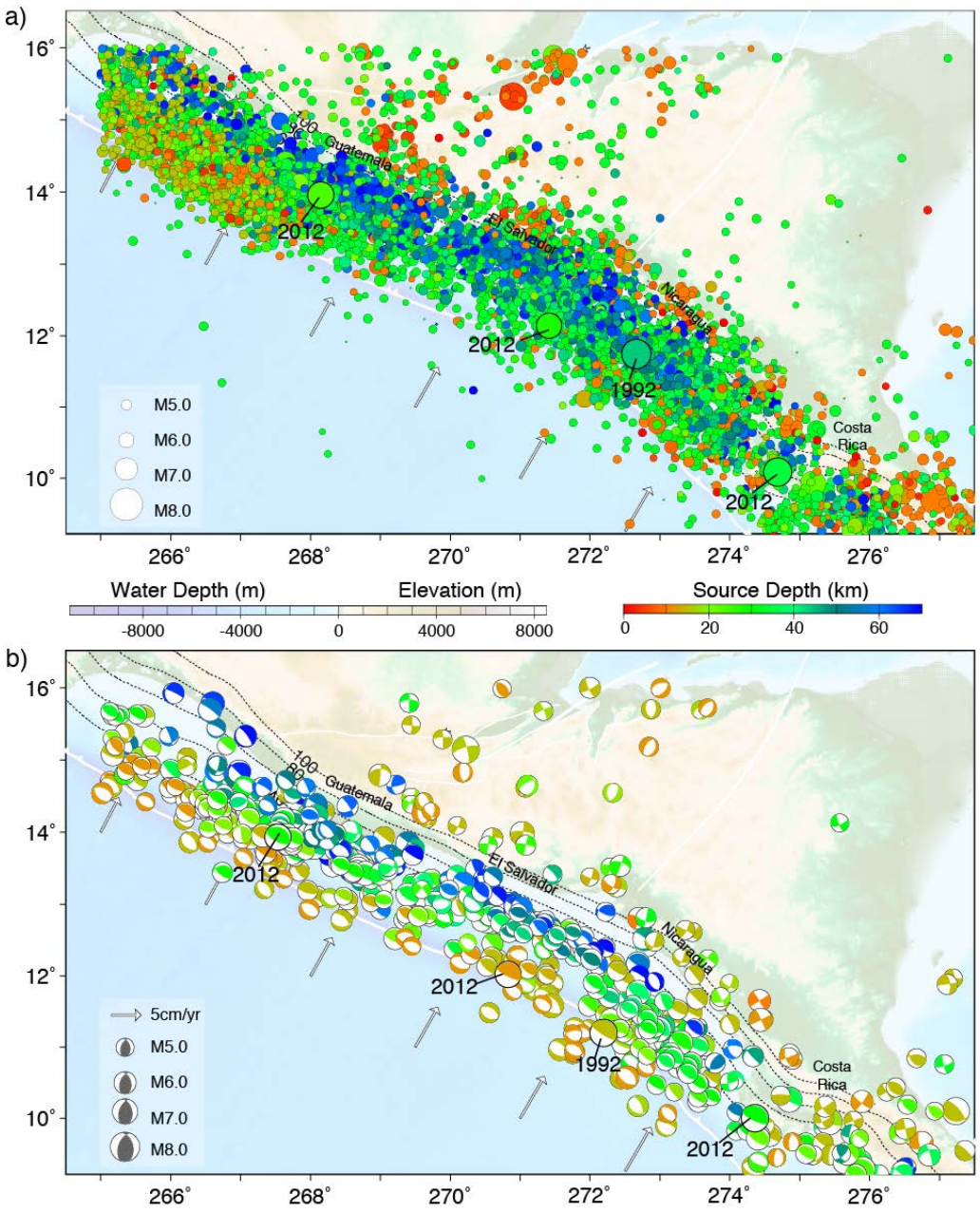

Figure S1. (a) Shallow seismicity along Middle America with $m_b \geq 5.0$ between 1973 and 2013 from the USGS/NEIC catalog. Symbol diameters are scaled with magnitude and colored by source depth. The epicenters of the November 7, 2012 Guatemala (M_w 7.4), August 27, 2012 El Salvador (M_w 7.3), September 2, 1992 Nicaragua (M_w 7.6), and September 5, 2012 Costa Rica (M_w 7.6) events are highlighted. The white curve indicates the position of the Middle America trench, and dashed lines show slab depth contours in km. The arrows show the estimated Cocos plate motion direction and rate relative to a fixed Caribbean plate computed using model NUVEL-1. (b) Best double-couple solutions from the Centroid-Moment Tensor catalog from 1976-2013 for events less than 70 km deep are plotted at the centroid locations. The symbol sizes are scaled relative to M_w. The mechanisms of the three events highlighted at the top are labeled.

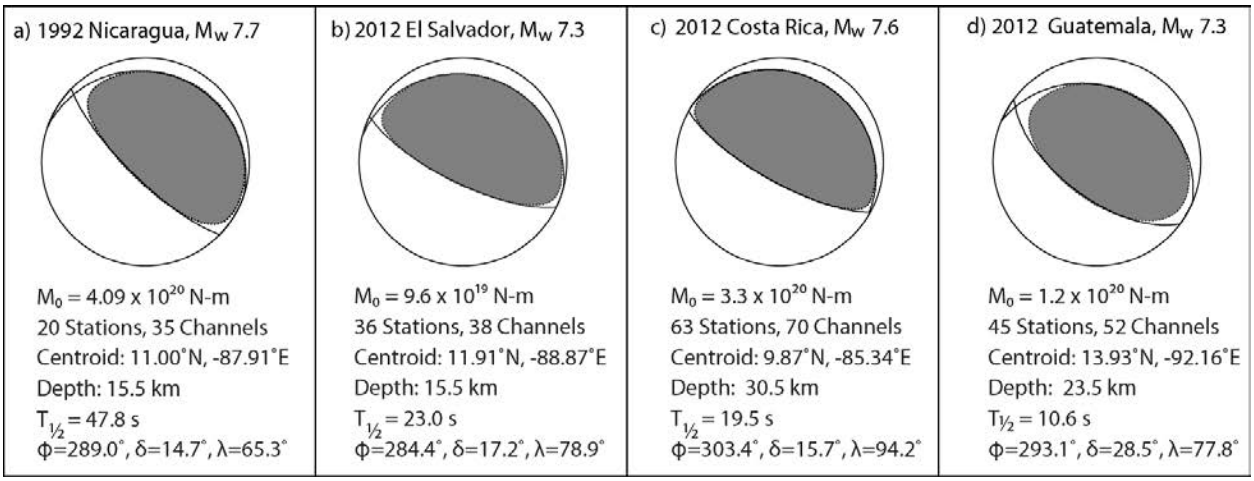

Figure S2. Point-source moment tensor from W-phase inversion for a) the September 2, 1992 Nicaragua event, b) the August 27, 2012 El Salvador event, c) the September 5, 2012 Costa Rica event and d) the November 07, 2012 Guatemala event. These solutions are for inversion of W-phase observations in the frequency band 1.67-5.0 mHz (200-600 s) from the indicated number of stations and channels, with the seismic moment (M_0), centroid epicenter and depth, centroid time shift ($T_{1/2}$) and strike (ϕ), dip (δ) and rake (λ) of the best double couple being given for each case. Observed and synthetic W-phase comparisons are shown in supplementary Figure S3.

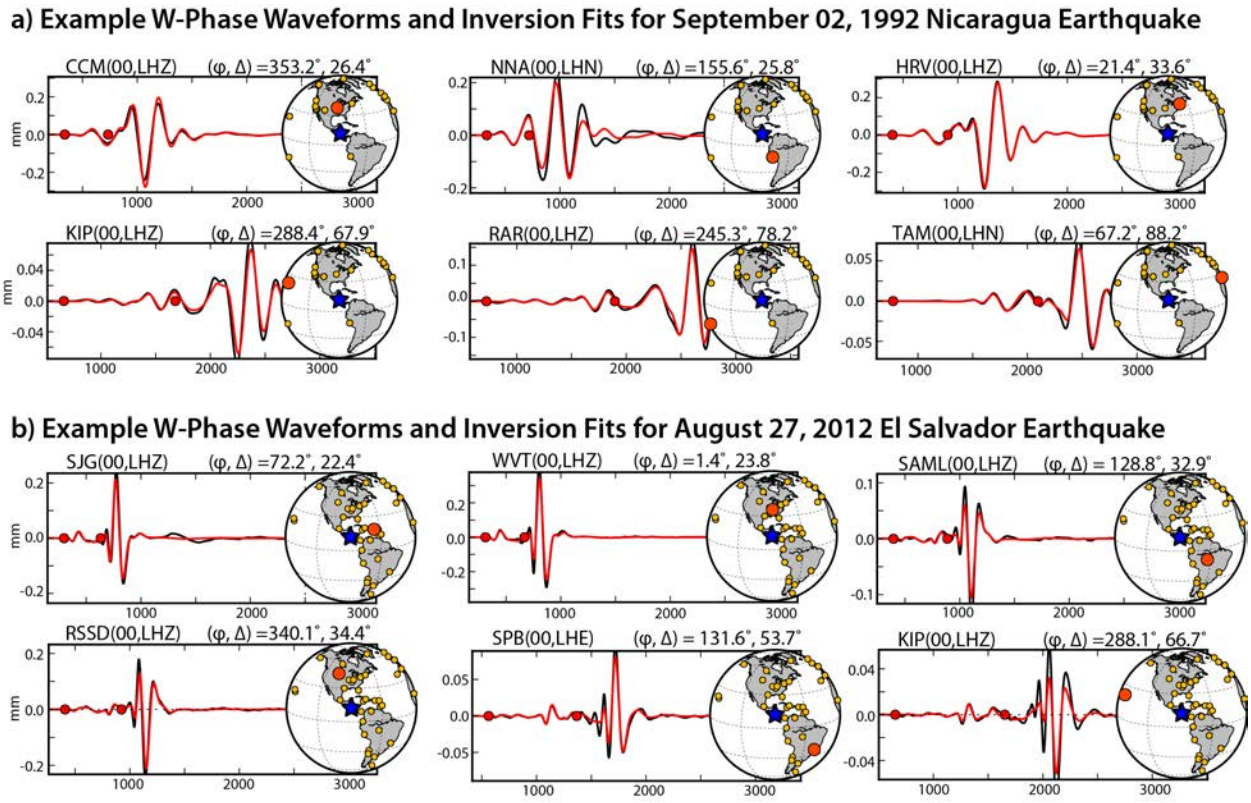

Figure S3. Example W-phase observations (black traces) and computed waveforms (red) for the point-source moment tensors in Figure S2 for a) the September 2, 1992 Nicaragua evetn, b) the August 27, 2012 El Salvador event, c) Costa Rica event and d) the November 7, 2012 Guatemala event. The data are from global seismic network stations with ground displacement filtered in the frequency band 1.67-5.0 mHz. The W-phase signal used in the inversions is the waveform interval between the red dots. The large amplitude signals after the W-phase are fundamental mode surface waves and the waveform comparisons are predictions for those signals. The maps indicate the position of the station (red dot) among the total set of stations (gold dots) used in the corresponding W-phase inversion.

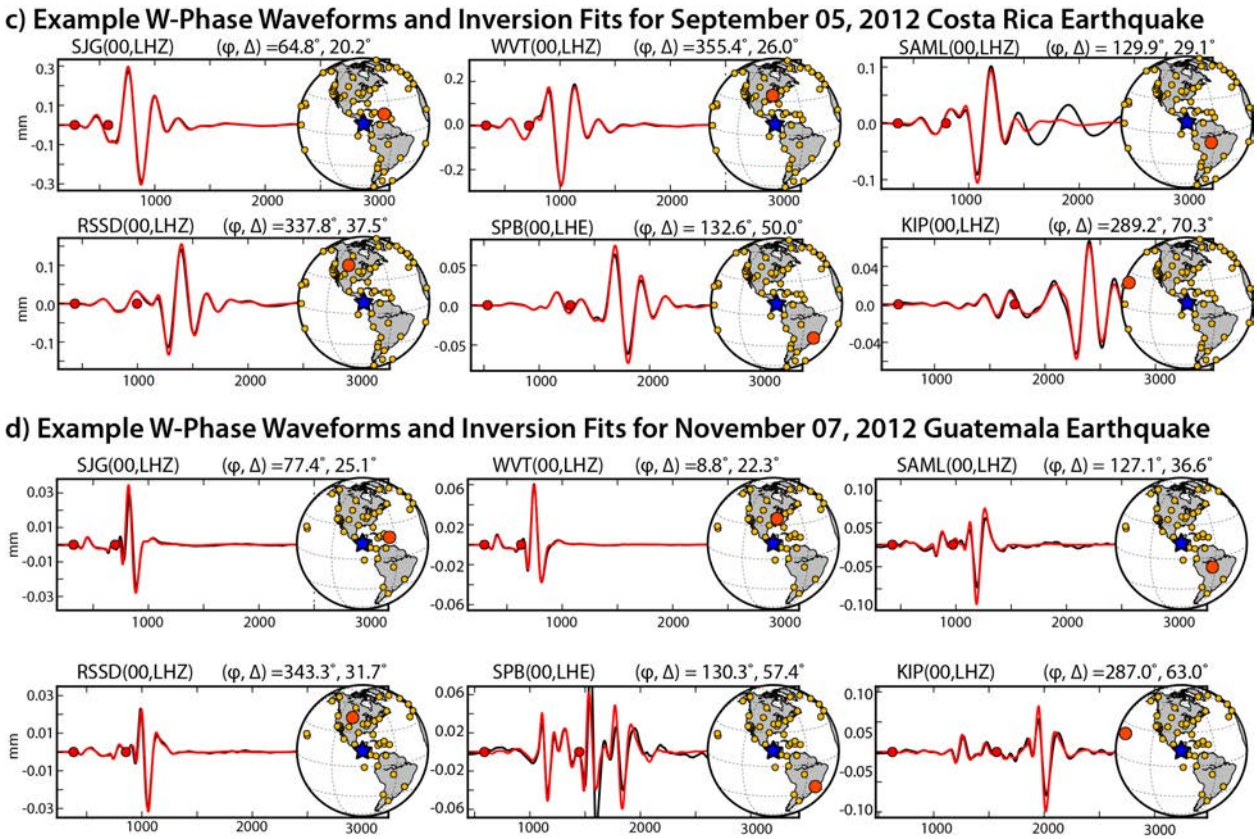

Figure S3. Continued.

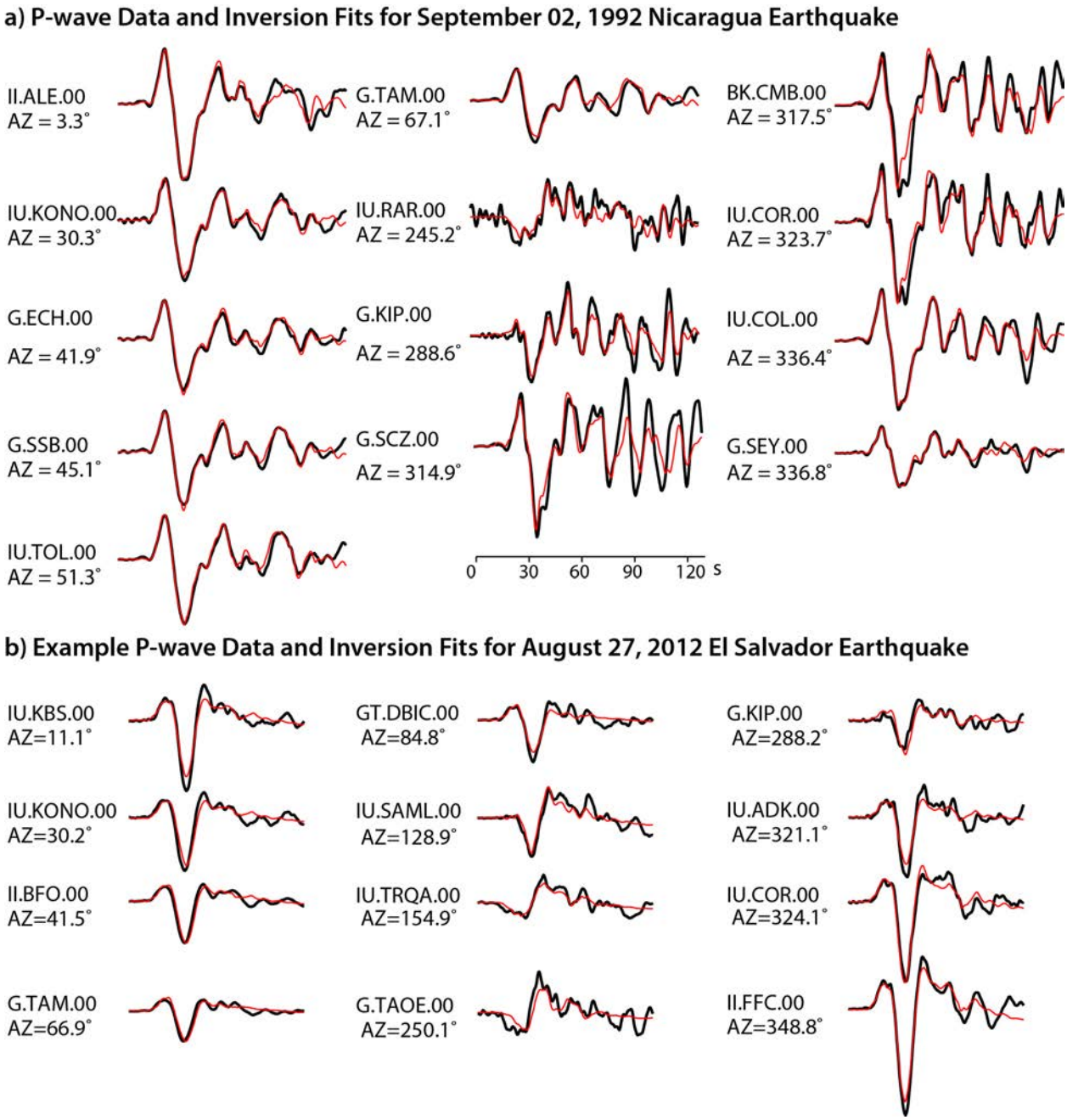

Figure S4. Comparison of representative observed (black lines) and modeled (red lines) teleseismic P waves for a) September 2, 1992 Nicaragua, b) August 27, 2012 El Salvador, c) September 5, 2012 Costa and d) November 7, 2012 Guatemala earthquakes. The models shown in Figure 2 are used for the computations. The signals are broadband ground displacements in the passband 0.005-0.9 Hz. Comparable waveform matches are found for all of the stations used in the inversions.

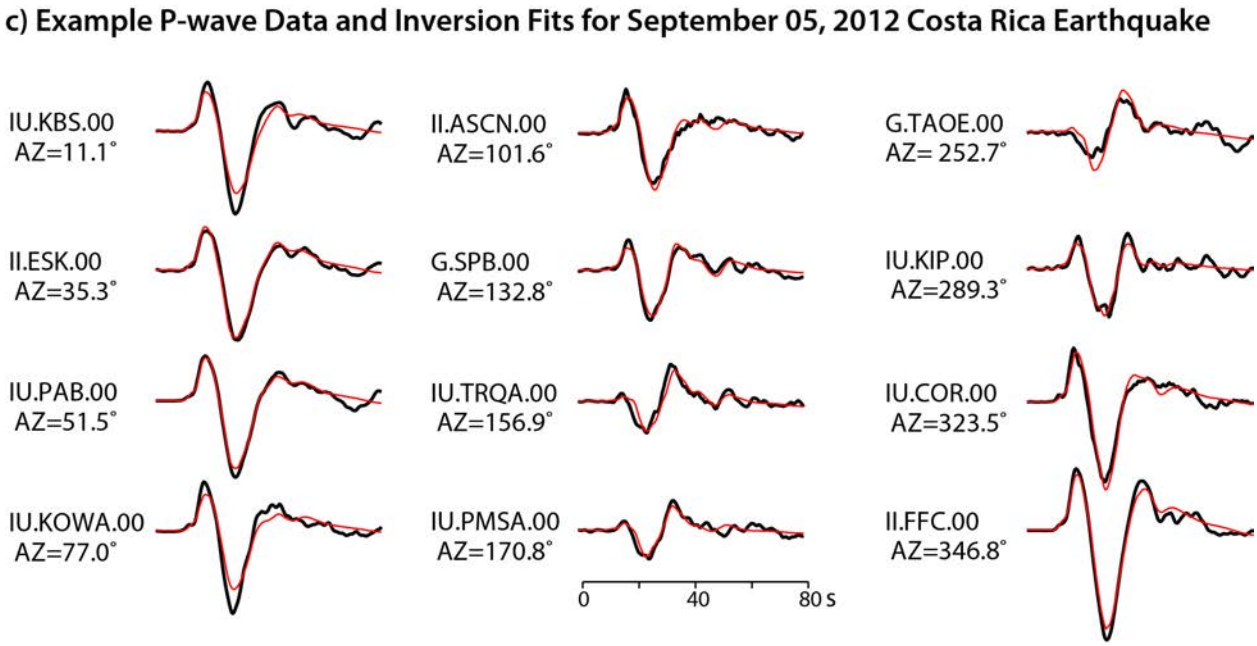

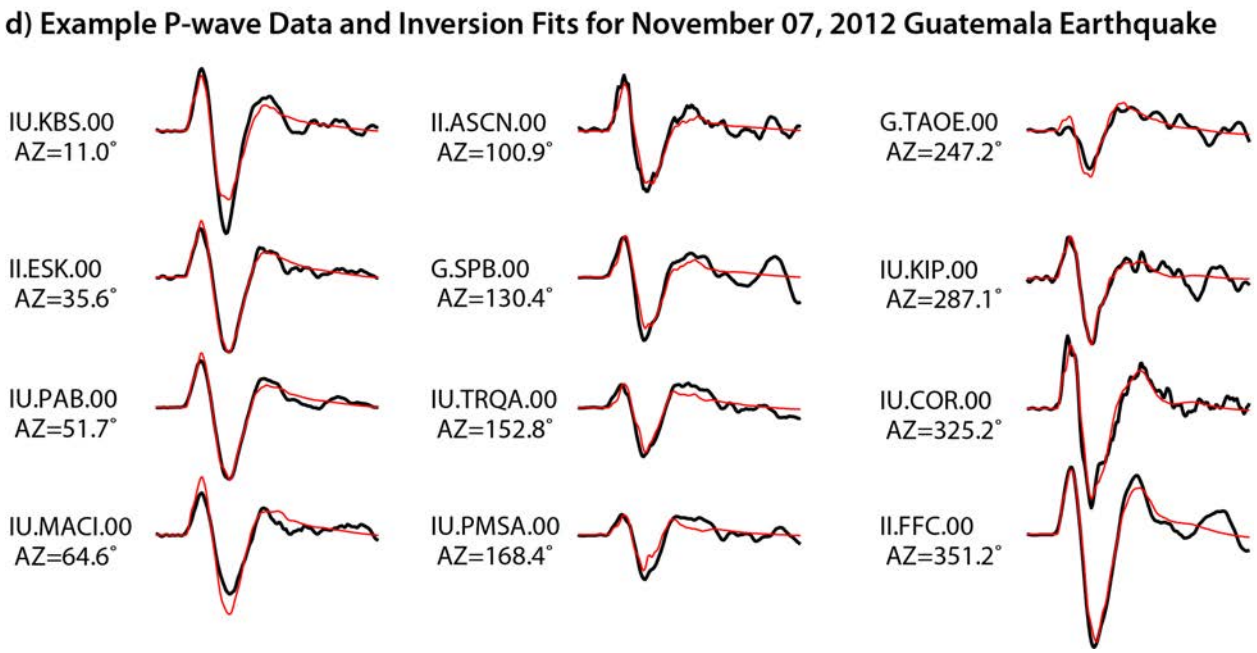

Figure S4. Continued.

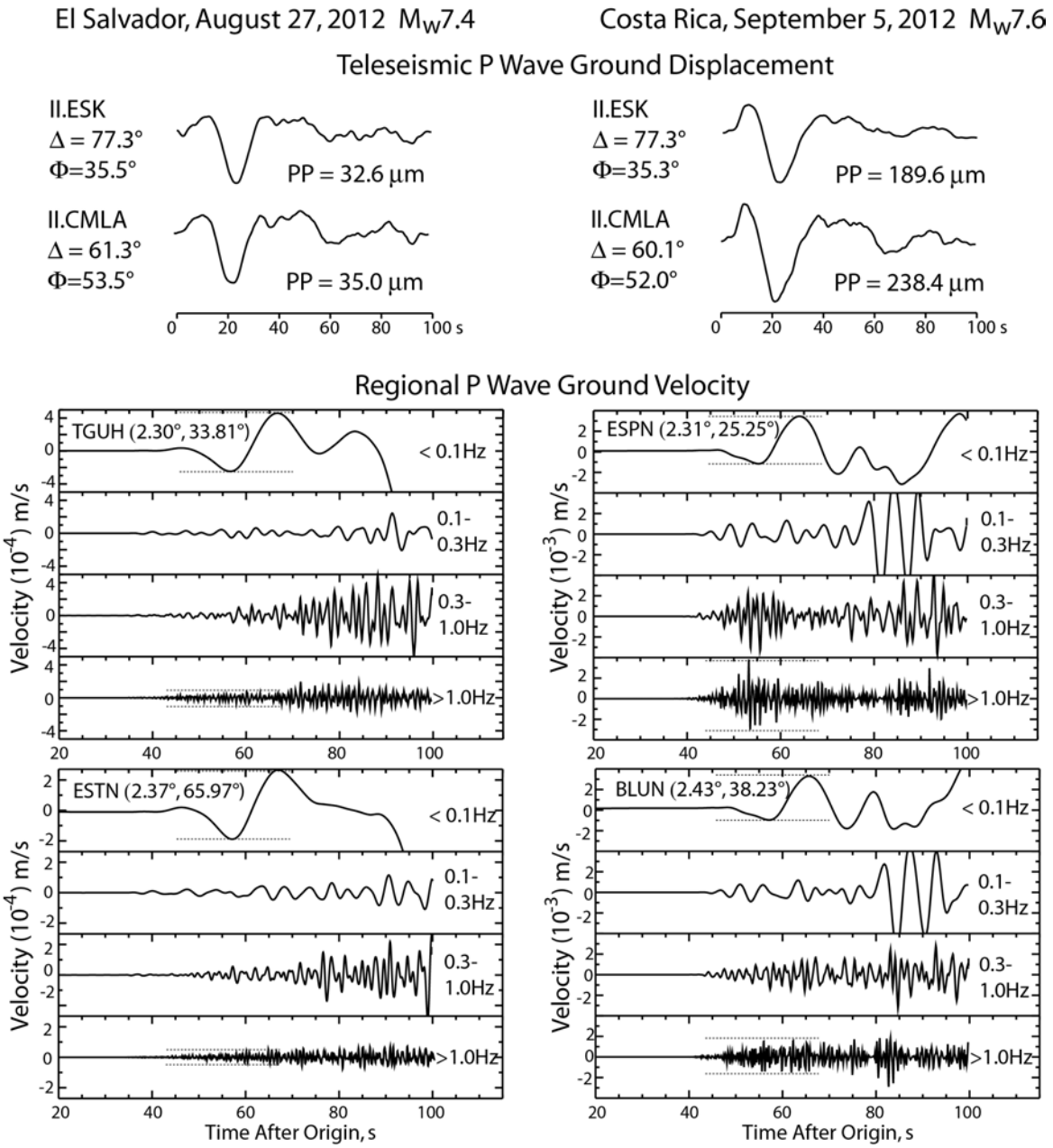

Figure S5. Comparison of teleseismic and regional P wave signals for the August 27, 2012 El Salvador (M_w 7.3) earthquake (left column) and the September 5, 2012 Costa Rica (M_w 7.6) earthquake (right column). The teleseismic P waves at common stations are not dramatically different in appearance, but the first arrival has more impulsive, short-period-rich onsets for the Costa Rica event. The spectral differences are more apparent in regional recordings at comparable propagation distances (station locations are shown in Figure 5), with narrow-band filtered ground velocities being shown below with true relative amplitudes. The ratio of the signal amplitudes in the P arrival for frequencies > 1 Hz relative to below 0.1 Hz is higher for the Costa Rica event by a factor of 3.6-5.6, consistent with the factor of 5 higher seismic moment-scaled radiated energy in Figure 4.

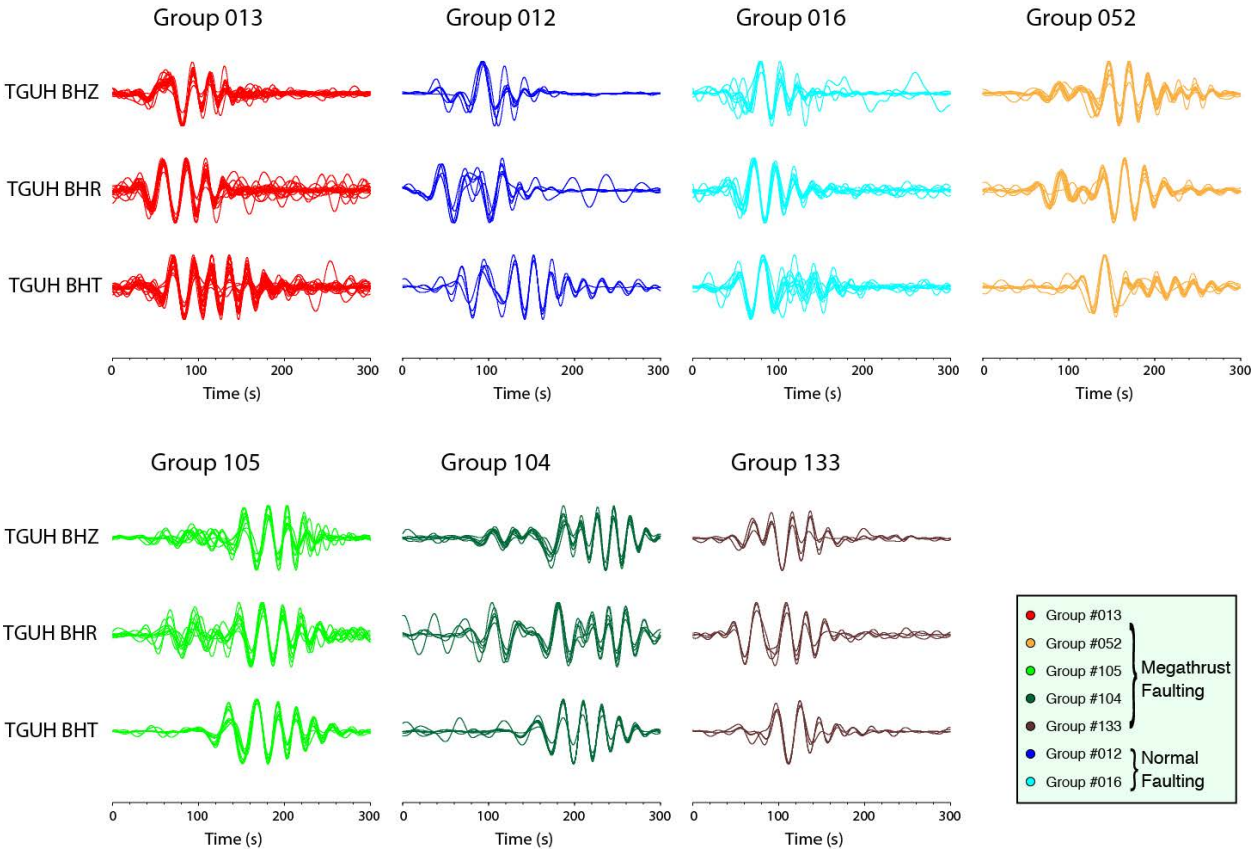

Figure S6. Aligned three-component 300-s long regional wave recordings at station TGUH that have been clustered by waveform correlations based on similarity to reference events 013, 012, 016, 052, 105, 104 and 133. The correlations are for waveforms band-passed in the frequency band 20 to 100 s for vertical components and 20 to 50 s for horizontal components. Amplitudes are normalized on the peak amplitude. Note the distinct waveform character for the different groups. The faulting geometry for each group is inferred using the gCMT solutions for the reference events.

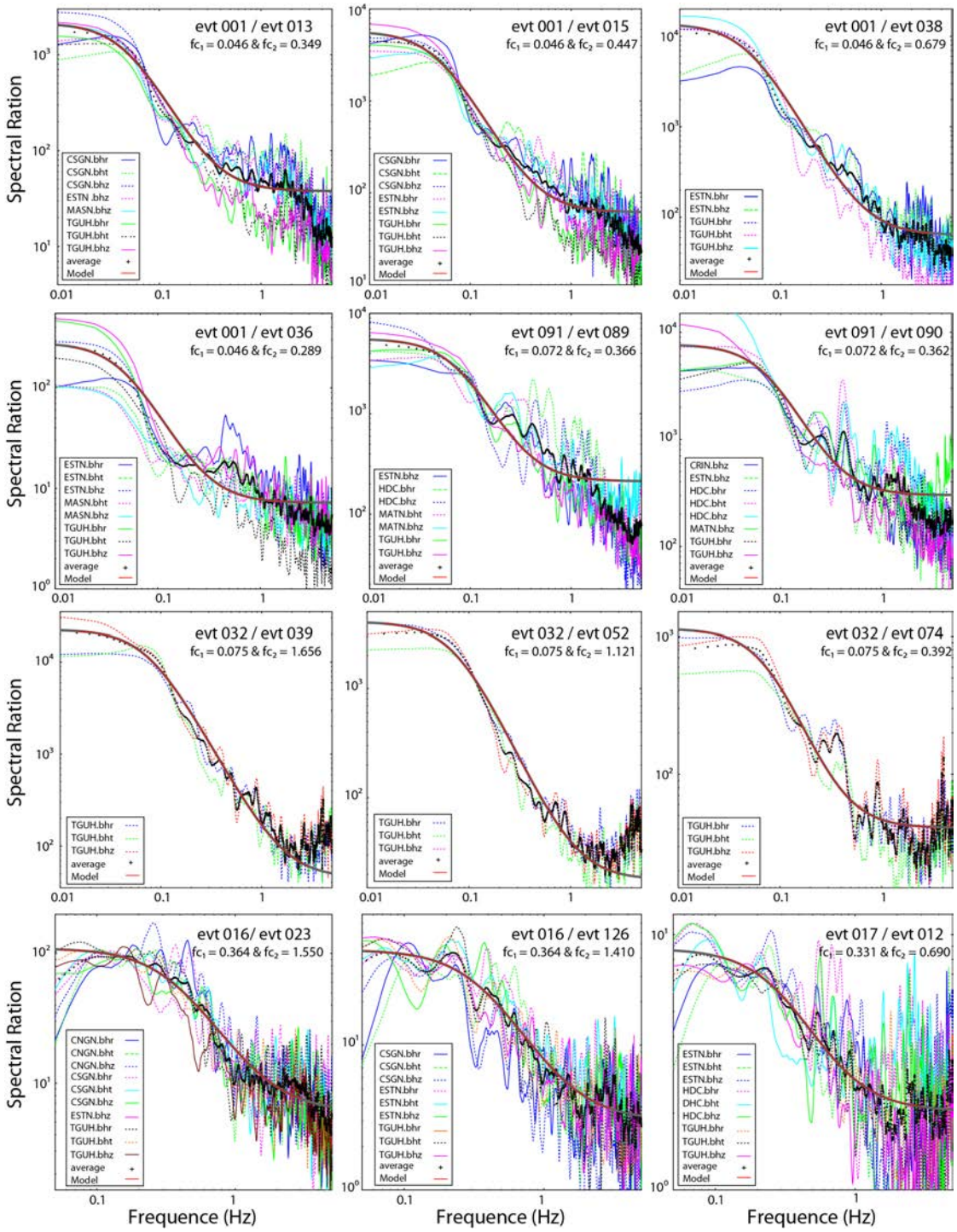

Figure S7. Example fitting of the stacked spectral ratios (heavy blank curves) between two nearby events (separation distance < 50 km) with similar focal mechanism using an ω^{-2} source model. 150-s-long signals after P arrivals are used and the individual spectral ratios (colors) used for calculating the average spectral ratios are indicated by the station name and component in each panel. The smooth curves show the best fitting spectral ratio (gray curves highlighted in red for the reliable frequency band used for fitting), with corner frequencies for denominator and numerator events being indicated by f_{c1} and f_{c2}.

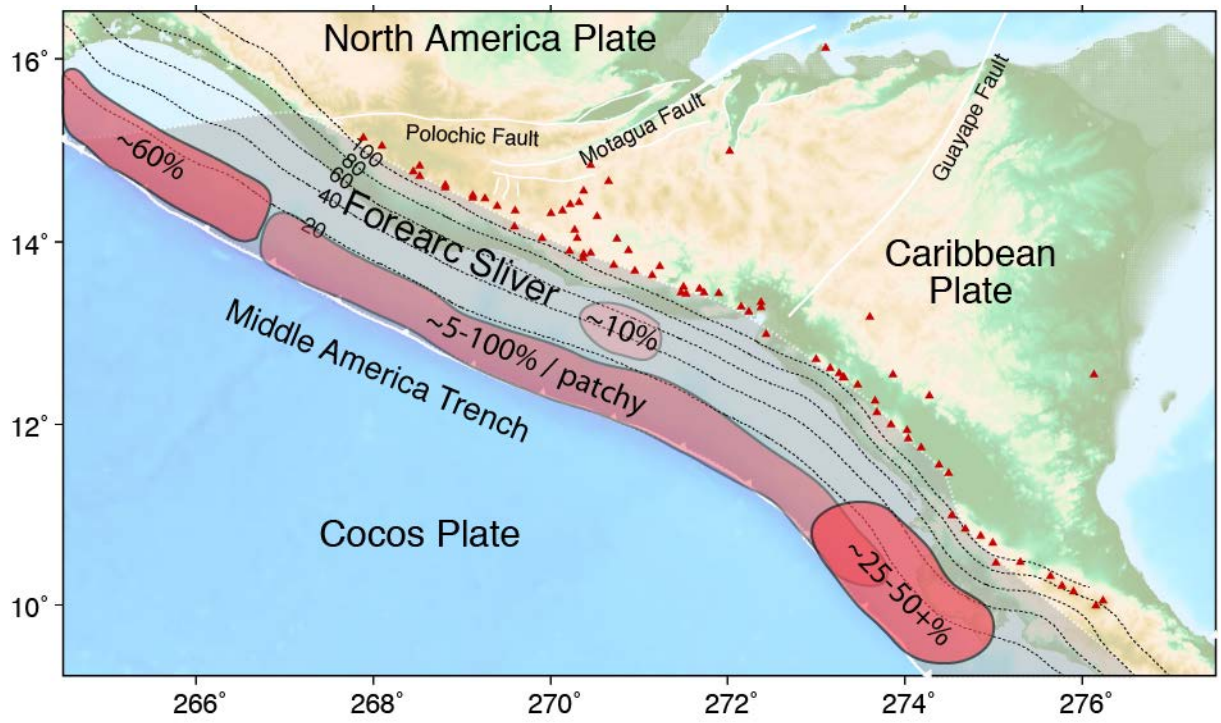

Figure S8. Map indicating inferences of megathrust locking based on several studies of GPS observations in Figure 7. The studies consistently indicate low or no coupling on the deeper portion of the megathrust below the forearc sliver, which is translating at about 15 mm/yr toward the triple junction of the North American, Cocos and Caribbean plates. Two patches with ~10% and ~25-50+% locking near El Salvador and Costa Rica, respectively are suggested by Correa-Mora *et al.* (2009) with less than 2% on average over the entire megathrust. Estimates ranging from 5 to 100% coupling for the shallow megathrust along the sliver extending to about 20 km depth have been proposed in various studies (LaFemina *et al*., 2009; Rodriguez *et al.*, 2009; Franco *et al*., 2012). Relatively strong locking of ~60%, near the triple junction has been proposed (Franco *et al*., 2012).